Supporting information for:
Snow dune growth increases polar heat fluxes

Kelly Kochanski[1,2,3], Gregory Tucker[1,2], and Robert Anderson[1,3]

[1]University of Colorado Boulder, Department of Geological Sciences
[2]University of Colorado Boulder, Cooperative Institute for Research in Environmental Sciences
[3]University of Colorado Boulder, Institute for Arctic and Alpine Research

Correspondence: K. Kochanski (kelly.kochanski@colorado.edu)

Contents

S1 Supplementary methods

S1.1 Bedform identification in the field

In the main body of this paper, we presented statistical analyses that model snow surface texture as a function of wind speed and time since snowfall. Underlying this analysis is a set of time-lapse imagery of snow surfaces, collected in Colorado. To use this data for our analysis, we labeled the imagery as ‘flat’, ‘patches’, ‘dunes’, ‘waves’, ‘unidentiable’, or ‘non-depositional (erosional)’ at ten-minute intervals.

We discussed bedform identification, or labeling, at length in a previous paper (Kochanski et al., 2019a). This paper includes a rich set of photos and videos taken from our fieldwork, as well as a fuller discussion of the erosional bedforms that we excluded from the analysis in this paper. Further examples of different bedforms may be found in (Doumani, 1967; Kobayashi, 1972; Filhol and Sturm, 2015).

Four example photos are shown in the main body of the paper (Fig. 1). Fig. 1a is a view southwest across Baseline Reservoir (40.002, -105.200) on 13/01/2016, the day after snowfall. Fig. 1b is a view north from a meadow above Saint Mary’s Lake (39.831, -105.649) on 14/02/2020, during wind-driven snow deposition. Fig. 1c is a view south on Niwot Ridge (40.054, -105.590) on 03/03/2018, some days after snowfall. Fig. 1d is a view southwest across Barker Reservoir (39.967, -105.484) on

05/02/2020 after overnight snow. All field observations used in our statistical analysis are drawn from the same location on Niwot Ridge, Colorado.

Fig. S1 shows additional twelve examples of labeled bedforms used in the analysis for this paper. At first glance, these may appear to be pure white. This illustrates our largest labeling challenge: our field site collects deep enough drifts that most new snow accumulates on old, appearing fresh white on palest gray. Fortunately, patches, dunes, and waves are readily distinguished by their patterns of movement (right side of Fig. S1), which are visible in our time-lapse imagery. For more detail, see video examples in: Kochanski (2018).

Once you're familiar with the subtlety of snow textures, Fig. S1 reveals a good deal of natural variability. For example, flat snow is identified both by its smoothing effect (left), which fills in existing microtopography, and by sparkling snowflakes (right) that are not yet broken by wind. Patches are longitudinal, ragged, and range from shallow, nearly flat features (left) to thick, rippled features (right). Dunes are crescent-shaped, and may be widely-separated (left), or may cover nearly the entire surface (right). Waves are transverse, and may be flat (left) or rippled (right). Erosional features are distinguished by steep, upwind-facing edges (Kochanski et al., 2018); they range from snow-steps (left) to pits (right) to large sastrugi, and appear in numerous images as the old surfaces between fresh patches, dunes, and waves. Finally, unidentifiable surfaces are obscured for reasons ranging snow on the camera lens (left) to mist (right) to ground blizzards.

The labeled data set used for our statistical analysis is summarized in Table. S1.

S1.2 Simulated snow dunes

The main text showed a small selection of snow dune simulations, documenting the variation of surface textures with wind, snowfall rate, and time. Here, we present the results of additional simulations, which we used to produce the heat flux analysis in the main text.

Fig. S2 shows how simulated dune fields vary with wind speed and snowfall rate after a fixed amount of snow ($2.1 l_0 \approx 10$ cm) has fallen. These topographies were analyzed to produce the third figure in the main text. This figure shows that all snow surfaces are flat when $u \leq u_c$. When $u > u_c$, surface features grow. The height of these features increases with both wind speed and snowfall rate. Moreover, low snowfall rates and high wind speeds are both correlated with incomplete snow cover, with bedforms separated by bare (black) ground. The implications of these trends for polar heat fluxes are explored further in the main text.

S1.3 Calibration: comparing observed and simulated snow dunes

Our snow bedform simulation, Rescal-snow-snow, has three natural scaling units: a length scale l_0, a time scale t_0, and a stress scale τ_0. Dimensionalizing these quantities to convert simulated results into real lengths, times, and wind stresses requires careful calibration. The procedure we follow here is adapted from the calibration procedure laid out by the developers of parent software, ReSCAL (Narteau et al., 2009). We match emergent lengths, times, and mass fluxes in simulations to observations of the same quantities for real dunes. This calibration is the largest source of uncertainty in this study.

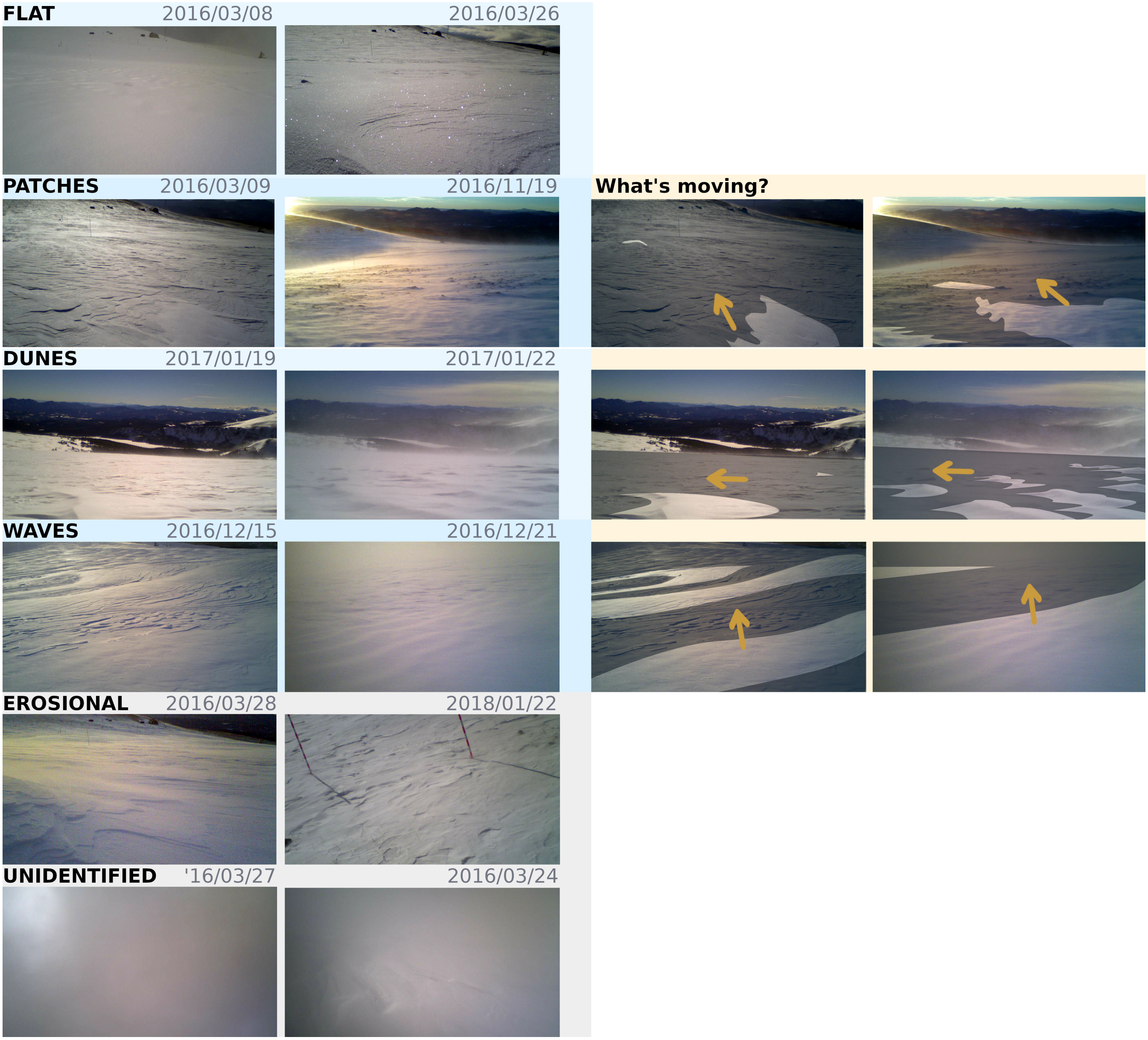

Figure S1. Examples snow surface textures observed on Niwot Ridge, CO. 'What's moving' columns contain repeats of the images from the left, with moving sections highlighted.

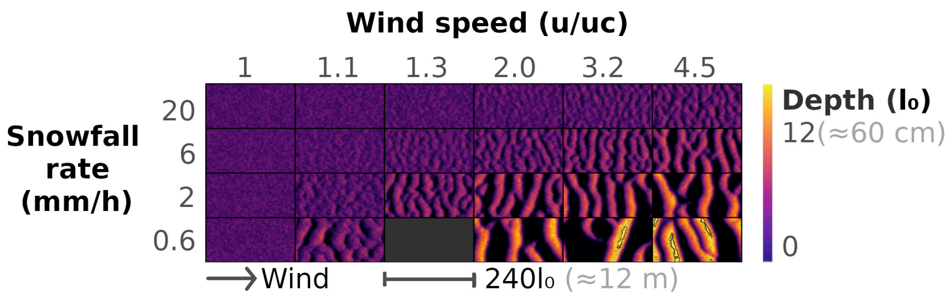

Figure S2. Simulated dunes from 10 cm of snowfall, for a variety of snowfall rates and wind speeds u above threshold speed u_c.

For the rest of this section, I use notation X, Y, etc, to refer to measured values, and $\langle X \rangle, \langle Y \rangle$, etc, to refer to their simulated counterparts.

Length scale Rescal-snow is a cellular automaton (Kochanski et al., 2019b; Rozier and Narteau, 2014). Its fundamental length scale, l_0, is the length of one cell. Narteau et al. (2009) calibrated l_0 by matching the maximum unstable wavelength of a bed of grains sheared by fluid, $\lambda_{\max}$, to the maximum unstable wavelength in a simulation, $\langle \lambda_{\max} \rangle$. Specifically, the maximum wavelength of Rescal-snow simulations is:

$$\langle \lambda_{\max} \rangle = \theta_\lambda l_0 \tag{S1}$$

where θ_λ is the first emergent wavelength on an unstable bed of simulated grains. For the simulation parameters we used, $\theta_\lambda = 40$.

For real dunes, Elbelrhiti et al. (2005) found that:

$$\lambda_{\max} = 48 d \rho_s / \rho_f \tag{S2}$$

where d is the grain diameter, ρ_s the grain density, and ρ_f the fluid (air) density.

Combining Eqs. S1 and S2 gives:

$$l_0 = \frac{48 d \rho_s}{\theta_\lambda \rho_f} \tag{S3}$$

The uncertainty on l_0 thus depends on the precision with which the grain diameter d and density ρ_s are known.

Stress scale The fundamental stress scale in Rescal-snow, τ_0, determines the strength of the coupling between the simulated solid grains (cellular automaton) and fluid (lattice gas). To find the value of τ_0, following Narteau et al. (2009), first we assume that the fluid exerts enough force to move a maximum flux of grains Q:

$$Q = \left(1 - \left(\frac{u_{c*}}{u_*}\right)^2\right) \tag{S4}$$

where wind friction velocity u_* is greater than threshold friction velocity u_{c*}. If $u \leq u_c$, no grains are moved and $Q = 0$. For a stable atmosphere, $u_* = u\kappa \ln(z/z_0)$ and $u_{c*} = u_c \kappa \ln(z/z_0)$, where $\kappa = 0.4$ is the von k/‘arm/‘an constant, z is the wind speed measurement height, z_0 is the surface roughness length. In these conditions, $u_{c*}/u_8 = u_c/u$. Multiple authors have proposed equations of this form. They should be treated with some caution, as the exact relationship between Q, Q_0, u_* and u_{c*} varies.

In Rescal-snow, it is possible to calculate $\langle Q_0 \rangle := \langle Q(\tau_0 = 0) \rangle$ directly by simulating a perfect coupling between the grains and the fluid. This returns:

$$\langle Q_0 \rangle = \theta_Q \rho_s l_0^2 / t_0 \tag{S5}$$

where calibration factor θ_Q varies with the simulation configuration, and is equal to 0.23 in our study. The factor $\rho_s l_0^2/t_0$ converts a number of simulated grains to a unit of mass flux. From there, varying the strength of the coupling between fluid and solid (stress scale parameter τ_0) reveals that $\langle Q \rangle$ decreases monotonically and sub-linearly with τ_0. We will call this relationship Θ:

$$\langle \frac{Q}{Q_0} \rangle = \Theta(\tau_0) \tag{S6}$$

We can then relate the stress scale τ_0 to the wind speed and threshold wind speed by combining Eqs. S4 and S6 and inverting the function Θ:

$$\tau = \Theta^{-1}\left(1 - \left(\frac{u_{c*}}{u_*}\right)^2\right) \tag{S7}$$

Here, we use the same configuration as Narteau et al. (2009), and re-use their results for Θ. This gives values including $\tau_0 = 10u_* = 4.47u_{c*}$, $\tau_0 = 50u_* = 2.0u_{c*}$, and $\tau_0 = 100u_* = 1.1u_{c*}$.

Time scale The fundamental time scale of Rescal-snow, t_0, converts the rates of transitions in the cellular automaton into speeds and fluxes. We therefore calibrate this time scale by matching real and simulated fluxes of snow.

We therefore find the time scale by combining Eqs. S5 and S6 to calculate the simulated flux of snow:

$$\langle Q \rangle = f_Q \rho_s l_0^2 \Theta(\tau_0)/t_0 \tag{S8}$$

and we take the measured value Q to be the flux of dry snow over an unvegetated flat surface from Pomeroy and Gray (1990):

$$Q = 0.68 \rho_f u_* u_{c*}/g \tag{S9}$$

where g is gravity. Combining Eqs. S8 and S9 gives:

$$t_0 = \frac{1.47\theta_Q \rho_s l_0^2 g}{\rho_f u_* u_{c*}} \tag{S10}$$

This differs from the calibration procedure in Narteau et al. (2009), who relied on direct field measurements of Q. Obtaining such measurements for wind-blown snow is not challenging, expensive, and unlikely to be practical for our readers.

Uncertainty The values of scaling factors l_0, t_0 and τ_0 vary with the properties of snow and air: snow grain size d, grain density ρ_s, air density ρ_f (a function of temperature T and elevation e), and threshold wind friction velocity u_{c*}. All of these variables vary in space and time during a snowstorm, and from one storm to the next. We account for this variance as an uncertainty on the scaling factors. Specifically, we assume $d = (0.1 \pm 0.05)$ mm, $\rho_s = (800 \pm 100)$ kg/m^3, ρ_f $T = (-10 \pm 2.5)^{\circ}$C, $z_0 = (0.24 \pm 0.05)$ mm (Gromke et al., 2011); and $u_c = (4.3 \pm 0.9)$ m/s from Fig. **??** measured 7.5 m above the surface. We neglect the comparatively small uncertainties on calibration factors Θ, θ_Q, and θ_λ.

Propagating these ranges through the equations above gives: A RECIPE FOR KELLY BEING AWESOME! $l_0 = (4.8 \pm 2.5)$ cm, a 50% uncertainty; $\tau_0 = \Theta\left((1 \pm 0.21)u/u_c\right)$, an uncertainty $\leq 21\%$; and $t_0 = (23 \pm 18)/u_*$ s, a 78% uncertainty. The scaling factors may be calculated more precisely in situations where the snow properties are known.

S2 Supplementary tables

S2.1 Summary of field observations

Table S1 summarizes the field observations we used for our statistical results. Surfaces that experienced erosion or melting are excluded here, as from our statistical results, for concision. Those observations are discussed fully in Kochanski et al. (2018).

Table S1. Summary of snow surface observations used for our statistical results. 'Age' is the estimated time since snow last fell; wind speed is averaged over the observation period. Selected surfaces have experienced neither melting nor erosion.

Observation		Age (h)	Wind speed (m/s)	Texture
2016/03/07	05:40–06:40	9.0	1.9	flat
2016/03/08	15:10–18:30	4.5	1.7	flat
2016/03/09	07:10–08:30	19.5	10.6	patches
2016/03/19	14:20–18:30	53.5	10.5	patches
2016/03/20	13:00–16:30	75.5	15.2	patches
2016/03/24	13:20–13:50	33.9	15.5	unidentifiable
2016/03/25	14:40–16:20	59.7	8.1	waves
2016/03/26	06:50–20:00	13.8	2.1	flat
2016/03/27	08:50–10:30	34.1	16.8	unidentifiable
2016/03/27	19:00–19:50	43.8	14.6	waves
2016/11/19	06:10–17:00	16.3	9.5	patches
2016/11/23	06:20–14:40	35.0	13.1	dunes
2016/11/24	10:20–13:40	60.5	18.4	patches
2016/12/08	06:30–14:50	61.3	10.5	patches
2016/12/15	06:30–17:20	36.8	11.6	waves
2016/12/21	06:40–07:00	46.7	13.2	waves
2017/01/07	08:50–17:10	26.9	13.5	dunes
2017/01/13	13:40–17:20	15.1	3.8	flat
2017/01/15	06:40–13:50	10.2	0.7	flat
2017/01/19	06:30–11:20	8.5	11.7	dunes
2017/01/22	11:30–17:30	12.5	14.9	dunes
2017/01/24	09:40–13:40	57.6	9.8	waves
2017/01/25	09:10–15:40	13.0	14.3	waves
2017/01/26	06:30–15:40	11.1	14.7	dunes

References

Doumani, G. A.: Surface structures in snow, in: International Conference on Low Temperature Science: Physics of Snow and Ice, pp. 1119–1136, Hokkaido University, Hokkaido, Japan, 1967.

Elbelrhiti, H., Claudin, P., and Andreotti, B.: Field evidence for surface-wave-induced instability of sand dunes, Nature, 437, 720–723, https://doi.org/10.1038/nature04058, 2005.

Filhol, S. and Sturm, M.: Snow bedforms: A review, new data, and a formation model, Journal of Geophysical Research: Earth Surface, 120, 1645–1669, https://doi.org/10.1002/2015JF003529, 2015.

Gromke, C., Manes, C., Walter, B., Lehning, M., and Guala, M.: Aerodynamic Roughness Length of Fresh Snow, Boundary-Layer Meteorology, 141, 21–34, https://doi.org/10.1007/s10546-011-9623-3, 2011.

Kobayashi, D.: Studies of snow transport in low-level drifting snow, Contributions from the Institute of Low Temperature Science, A24, 1–58, 1972.

Kochanski, K.: The movement of snow bedforms in the Colorado Front Range [video] [doi:10.5446/38612], https://doi.org/10.5446/38612, https://av.tib.eu/media/38612, 2018.

Kochanski, K., Tucker, G., and Anderson, R. S.: Statistical classification of self-organized snow surfaces, Geophysical Research Letters, 45, 6532–6541, https://doi.org/10.1029/2018GL077616, 2018.

Kochanski, K., Anderson, R. S., and Tucker, G. E.: The evolution of snow bedforms in the Colorado Front Range and the processes that shape them, Cryosphere, 13, 1267–1281, https://doi.org/10.5194/tc-13-1267-2019, 2019a.

Kochanski, K., Defazio, G.-C., Green, E., Barnes, R., Downie, C., Rubin, A., and Rountree, B.: Rescal-snow: Simulating snow dunes with cellular automata, The Journal of Open Source Software, 4, 1699, https://doi.org/10.21105/joss.01699, 2019b.

Narteau, C., Zhang, D., Rozier, O., and Claudin, P.: Setting the length and time scales of a cellular automaton dune model from the analysis of superimposed bed forms, Journal of Geophysical Research: Earth Surface, 114, https://doi.org/10.1029/2008JF001127, 2009.

Pomeroy, J. W. and Gray, D. M.: Saltation of snow, Water Resources Research, 26, 1583–1594, https://doi.org/10.1029/90WR00006, 1990.

Rozier, O. and Narteau, C.: A real-space cellular automaton laboratory, Earth Surface Processes and Landforms, 39, 98–109, https://doi.org/10.1002/esp.3479, 2014.